JOURNAL OF SOLID STATE CHEMISTRY **140,** 226–232 (1998)
ARTICLE NO. SC987880

Ta_3SBr_7—A New Structure Type in the M_3QX_7 Family (M = Nb, Ta; Q = S, Se, Te; X = Cl, Br, I)

Mark Smith and Gordon J. Miller[1]

Department of Chemistry, Iowa State University, Ames, Iowa 50011-3111

Received November 25, 1997; in revised form May 5, 1998; accepted May 12, 1998

The layered compound Ta_3SBr_7 has been prepared by direct reaction of the elements at 550°C for 2 weeks in evacuated Pyrex ampules, and its structure determined by single-crystal X-ray diffraction. Ta_3SBr_7 crystallizes with monoclinic symmetry in space group *Cm*; $a = 12.249(2)$ Å, $b = 7.071(2)$ Å, $c = 8.829(2)$ Å, $\beta = 134.421(8)°$, $V = 546.16(23)$ Å^3, $Z = 2$, $R = 0.027$, $R = 0.032$. The structure, related to the $Cd(OH)_2$ type, consists of triangular tantalum clusters located between every other layer of a closed-packed mixed S/SBr ordered anion framework. The slightly distorted, quasi-infinite $^2_\infty[Ta_3SBr_7]$ slabs stack parallel to the crystallographic *ab* plane in a new variant, with each successive $^2_\infty[Ta_3SBr_7]$ slab related by a 1/2b+c stacking vector. This stacking mode is the sixth layered structure type observed in the M_3QX_7 system. Ta_3SBr_7 represents the first Ta_3QX_7 compound discovered that is not isostructural with its niobium counterpart and is the second of the two one-slab per unit cell stacking types possible in the M_3QX_7 system Nb_3SBr_7 being the other. Synthesis, structural characterization, and lattice energy calculations of Ta_3SBr_7 and related compounds are reported.

INTRODUCTION

In 1998, as part of an investigation of the potentially rich ternary niobium–chalcogen–halide system, Hönle and Furuseth synthesized Nb_3TeBr_7 by reaction of Nb metal, $NbBr_5$, and Te at 800°C (1), the first of a series of niobium chalcogenide halides with this composition to be prepared. Subsequently, all Nb_3QX_7 members (Q = S, Se,Te; X = Cl, Br, I) have been reported (2). Nb_3QX_7 crystallize with structures similar to those of the binary niobium halides Nb_3X_8 (X = Cl, Br, I), which are themselves derivatives of the $Cd(OH)_2$ type.[2] In Nb_3X_8, layers of close-packed halide ions are interleaved by Nb atoms, which order in $\frac{3}{4}$ of the octahedral sites between every other layer. The relationship of these structures to that of $Cd(OH)_2$ is seen by removing $\frac{1}{4}$ of the Cd atoms and drawing the remaining occupied metal sites together into M–M bonded triangular clusters. Nb_3X_8 can therefore be formulated $Nb_3(\text{vacancy})_1X_8$. The local metal cluster unit is the common M_3X_{13} type, formulated in the notation of Schäfer and von Schnering as $M_3(\mu_3 - X^i)(\mu_2 - X^i)_3(\mu_3 - X^a)_3(\mu_2 - X^a)_6$. The triangular metal cluster has one μ_3 capping atom, three μ_2 edge-bridging atoms, and nine atoms which provide bridges to other clusters and link the extended layers together. Electronically, the binary halides have seven electrons per Nb_3 cluster unit, resulting in an unpaired electron and giving rise to paramagnetic behavior. Substitution of a chalcogen into these binary halides results in a one-electron oxidation of the cluster and leads to the ternary series Nb_3QX_7, with formally six-electron, closed-shell configurations, and diamagnetic behavior. In all Nb_3QX_7 cases, the chalcogen acts as the μ_3 cluster-capping atom. This has been explained on the basis of site electron density and electronegativity (3).

This family of layered compounds can be viewed as stacked $^2_\infty[Nb_3QX_7]$ slabs separated by a van der Waals gap. With essentially limitless ways to stack the $^2_\infty[Nb_3QX_7]$ slabs, and two possible orientations of the Nb_3Q_{cap} fragment, there exists the potential for polytypism. To date, six structure types have been discovered in the closely related Nb_3X_8/Nb_3QX_7 systems: α-Nb_3Cl_8 (4), β-Nb_3I_8 (5), Nb_3SeI_7 (1), Nb_3TeBr_7 (1), Nb_3SBr_7 (6), and o-Nb_3SI_7 (7). The details of the stacking patterns of all these have been summarized previously (2). All have trigonal or hexagonal symmetry reflecting the 3-fold symmetry of the metal cluster unit, except the orthorhombic compound o-Nb_3SI_7, which displays undulating $^2_\infty[Nb_3SI_7]$ layers featuring $[Nb^a_3S^{i-a}_{1/2}I^i_3(I^a_{2/2}S^{a-i}_{1/2})I^a_{6/2}]$ clusters.

The motivation for extending this chemistry to tantalum is evident when realizing that Ta_3X_8 have been never been reliably reported, and that until recently there was no example of a trinuclear Ta cluster made by high-temperature solid state methods. We have recently prepared Ta_3SeI_7 and Ta_3TeI_7 (8), the tantalum analogues of Nb_3QI_7

[1]To whom correspondence should be addressed.

[2]The $Cd(OH)_2$ structure type is often referred to as the CdI_2 type. However, CdI_2 forms several stacking variants, while $Cd(OH)_2$ forms just one. To specify the structure exactly, $Cd(OH)_2$ is used here.

0022-4596/98 $25.00

(Q = Se, Te), and now report Ta_3SBr_7, a new stacking variant and structure type in the M_3QX_7 family.

EXPERIMENTAL

Synthesis

Polycrystalline Ta_3SBr_7 was synthesized by stoichiometric reaction of the elements in evacuated, flame-dried Pyrex tubes at 550°C for 2 weeks. Small strips of tantalum foil (Aesar, 99.95%) were washed with a concentrated HF/HNO_3/H_2SO_4 solution to remove surface impurities and then dried in vacuo at 1000°C. Sulfur (Alfa) was sublimed before use. The Ta strips and the sulfur powder were loaded into the reaction ampule in an Ar-filled glovebox and were then taken out and attached to a vacuum line for transfer of Br_2. Bromine (Fisher) was deoxygenated by several freeze–pump–thaw cycles before it was distilled onto P_2O_5 for drying and storage; subsequently the appropriate amount of Br_2 was vacuum-transferred from its volumetric storage tube directly into the reaction ampoule containing Ta and S_8. This mixture (Ta foil and a garnet-red liquid of presumably $Br_2 + S_2Br_2$) was frozen solid with liquid nitrogen, evacuated to ca. 10^{-3} Torr, and flame-sealed under vacuum. The tube (10 cm × 8 mm i.d.) was then placed in a horizontal tube furnace packed with asbestos to smooth out temperature gradients, and heated to 550°C for 12 days. The product from this step was a coarse-textured black solid that ground with a lubricating feel, and a small amount of orange $TaBr_5$. Subsequently, the black solid was ground to a fine powder in an Ar-filled glovebox and loaded into another Pyrex tube, evacuated and sealed, and placed in a 505–495°C temperature gradient. After 6 weeks, several small clumps of black, reflective, dagger-shaped crystals were found throughout the tube, but predominantly at the hot end. The majority of the product remained powdered.

Structure Solution

A small black dagger crystal was epoxied in air onto a thin glass fiber, and, after an initial crystal-quality check using the Weissenberg technique, aligned on a Siemens P4 diffractometer. (Crystals of Ta_3SBr_7 appear to be air- and moisture-stable for at least several weeks.) The initial unit cell and symmetry of Ta_3SBr_7 were determined on the basis of six reflections taken from a rotation photograph. Subsequently 40 reflections of varying intensities located between 22 and 25° in 2θ were used to refine the cell. Axial photographs were taken of all three axes to verify the unit cell lengths. Due to its small size, the crystal was then moved to a Rigaku AFC6R diffractometer to take advantage of the greater intensity offered by the rotating anode instrument. 1118 data were collected with no centering restrictions, of which 509 were observed ($I > 3\sigma_I$). Systematic absences confirmed a C-centered lattice and positively ruled out a c-glide operation, leaving three space groups; $C2$, $C2m$, and Cm. Of these, $C2m$ was discounted on the basis of intensity statistics, which strongly indicated noncentrosymmetry. Initially, the space group Cm was chosen, and the structure was solved by direct methods (9). All atoms were easily located based on Fourier map peaks, reasonable Ta–Ta, Ta–S, and Ta–Br distances, and structural similarities of Ta_3SBr_7 to other M_3QX_7 compounds. Subsequent failed attempts to solve the structure in $C2$, along with the noncentrosymmetric nature of the structure (see structure discussion below), verified the space group assignment. ψ scans of six reflections were averaged and applied to the data to correct for absorption, and, after isotropic refinement (10), a DIFABS correction was applied (11). All atoms were then refined anisotropically. The final residuals converged at $R = 0.027$, $R_w = 0.032$. Further crystallographic information is listed in Table 1. Atomic coordinates and anisotropic displacement parameters are given in Table 2. Tables of observed and calculated structure factors are available from the authors.

TABLE 1
Crystallographic Data for Ta_3SBr_7

Formula weight	1134.23
Crystal system	Monoclinic
Space group	Cm (No. 8)
Color of crystal	black
Dimensions of crystal (mm)	0.03 × 0.04 × 0.2
Lattice parameters	
a (Å)	12.249(2)
b (Å)	7.071(1)
c (Å)	8.829(2)
β (deg)	134.421(8)
Vol. (Å^3)	546.16(23)
Z	2
d_{calc} (g cm^{-3})	6.896
Diffractometer	Rigaku AFC6R (Mo$K\alpha$)
Linear absorption coefficient	55.13 mm^{-1}
Transmission ranges	0.87–1.0
Temperature of data collection	23°C
Scan mehtod	2θ–ω scan
Range in hkl	$h, k, \pm l$
$2\theta_{max}$ (deg)	50
No. of reflns. measd	1118
No. of unique reflns.	1067
No. of unique reflns observed ($I > 3\sigma_I$)	509
R (int)	0.1193
No. of parameters refined	57
Largest ΔF peak, e/Å^3	2.0
Residuals[a]	
R	0.0267
R_w	0.0322

[a] $R = \sum||F_o| - |F_c||/\sum|F_o|$; $R_w = [\sum w(|F_o| - |F_c|)^2/\sum w(F_o)^2]^{1/2}$; $w = 1/\sigma^2(F_o)$.

TABLE 2
Atomic Coordinates and Isotropic and Anisotropic Displacement Parameters for Ta_3SBr_7

Atom	Position	x	y	z	B_{eq}[a]
Ta1[b]	2*a*	0.9643	0	0.6138	0.65(6)
Ta2	4*b*	0.1662(2)	0.2025(1)	0.6129(3)	0.63(4)
Br1	2*a*	0.6553(7)	0	0.393(1)	0.8(2)
Br2	2*a*	0.7111(7)	0	0.8380(8)	1.0(2)
Br3	2*a*	0.1327(7)	0	0.3444(8)	1.1(2)
Br4	4*b*	0.9638(5)	−0.2537(8)	0.8384(6)	1.0(1)
Br5	4*b*	0.8799(5)	−0.2539(8)	0.3454(5)	1.0(1)
S	2*a*	0.243(2)	0	0.886(2)	0.7(4)

Atom	U_{11}[c]	U_{22}	U_{33}	U_{12}	U_{13}	U_{23}
Ta1	0.009(1)	0.0087(8)	0.010(1)	0.0	0.0075(9)	0.0
Ta2	0.0088(6)	0.0074(5)	0.0112(6)	−0.0012(6)	0.0082(5)	−0.0007(6)
Br1	0.013(3)	0.011(3)	0.016(2)	0.0	0.013(2)	0.0
Br2	0.021(3)	0.010(3)	0.013(2)	0.0	0.014(3)	0.0
Br3	0.019(3)	0.013(3)	0.018(3)	0.0	0.016(3)	0.0
Br4	0.011(2)	0.014(2)	0.014(2)	0.005(2)	0.009(2)	0.0058(6)
Br5	0.011(2)	0.013(2)	0.014(2)	−0.006(2)	0.009(2)	−0.0069(5)
S	0.009(7)	0.009(6)	0.015(6)	0.0	0.010(6)	0.0

[a] $B_{eq} = (8\pi^2/3)\sum_i\sum_j U_{ij}a_i^*a_j^*\mathbf{a}_i\mathbf{a}_j$.
[b] Ta1 positional parameters fixed in x, z.
[c] $U_{ij} = \exp(-2\pi^2(a^{*2}U_{11}h^2 + b^{*2}U_{22}k^2 + c^{*2}U_{33}l^2 + 2a^*b^*U_{12}hk + 2a^*c^*U_{13}hl + 2b^*c^*U_{23}kl))$.

Theoretical Calculations

Lattice energy calculations were performed on several possible Ta_3SBr_7 stacking variants. The calculations included two terms: the Madelung energy, U_{MAD}, and the Born–Mayer repulsion energy, U_{BM}, which can be expressed as follows:

$$U_{MAD} = 14.40 \sum_{ij} q_i q_j / r_{ij}, \qquad [1]$$

$$U_{BM} = b \sum_{ij} (1 + q_i/r_i(0) + q_j/r_j(0)) \exp(-r_{ij}/\rho). \qquad [2]$$

Summations were carried out over all pairs of atoms $\{ij\}$ except when $i = j$. The scale factor b in the Born–Mayer term is determined by assuming the lattice energy calculated for each structure to be a minimum with respect to the shortest anion–cation distance R_0, i.e., $(\partial U_{LAT}/\partial R)|_{R=R_0} = 0$. As discussed later, twelve separate structures were investigated. Since the scale factors for all twelve were nearly identical, an average value was calculated and used for all twelve. $r(0)$ values are the "basic radii" for ions as defined by Bevan and Morris (12). These values are Ta, 0.72 Å; S, 1.84 Å; Br, 1.96 Å. Finally, $\rho = 0.345$ Å. The Madelung energy was evaluated using the Ewald method (13).

RESULTS AND DISCUSSION

Ta_3SBr_7 crystallizes in a new structure type, and is the first Ta compound in the M_3QX_7 system not isostructural with its Nb counterpart. However, the basic structural motifs present in Ta_3SBr_7 are quite similar to other M_3QX_7 compounds. Figure 1 shows an approximate [010] view of the Ta_3SBr_7 structure, with the unit cell and anion sheet stacking sequence indicated. Ordered, nearly close-packed mixed-anion sheets pack in an $\ldots AB\ldots$, or $\ldots h\ldots$, fashion, the same general anion stacking pattern observed in Nb_3SBr_7. The sulfur atoms occur only in every other mixed-anion layer (the "B" layer in Fig. 1), and order in a hexagonal pattern commensurate with the location of the metal clusters. This ordering pattern is shown in Fig. 2. Tantalum atoms reside in $\frac{3}{4}$ of the octahedral holes in alternate layers, and cluster together to form the trinuclear clusters that hallmark all M_3QX_7 compounds. The Ta_3 clusters are always situated directly beneath, and so are capped by, the sulfur atoms. In Ta_3SBr_7, all of these Ta_3S "tetrahedra" are oriented in the same direction throughout the structure, an arrangement which automatically precludes centrosymmetry.

As noted above, in both Nb_3SBr_7 and Ta_3SBr_7 the mixed anion layers pack in an $\ldots AB\ldots$ ($\ldots h\ldots$) fashion, with one $^2_\infty[M_3SBr_7]$ slab per unit cell. However, because of the presence of the triangular metal clusters, coupled with the sulfur-bromine ordering in the anion layers, a shift in the stacking of successive $^2_\infty[Ta_3SBr_7]$ slabs causes the adoption of the new structure type in the tantalum system while maintaining the same general anion layer stacking sequence found in Nb_3SBr_7. In fact, as discussed in more detail later in this paper, the Nb_3SBr_7 and Ta_3SBr_7 structure types represent the only two unique ways to stack M_3QX_7 type slabs while maintaining one slab per unit cell. The construction of these two types is now described: Fig. 3 shows one $^2_\infty[M_3QX_7]$ slab viewed down the stacking direction. The large dark circles constitute an "A" anion sheet, and the large open circles a "B" sheet. The unique atom (S) at the centers of the hexagonal spaces formed by the surrounding anion matrix are labeled, and the metal

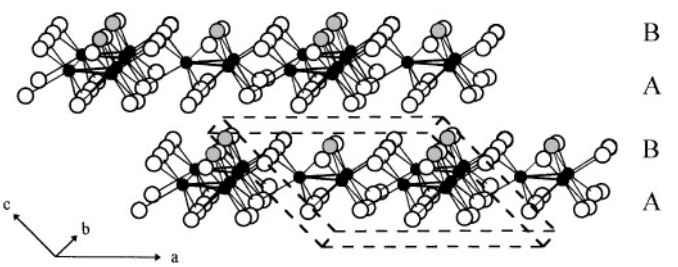

FIG. 1. Approximate [010] view of Ta_3SBr_7, with the unit cell. The mixed-anion sheet stacking sequence is indicated also. Black circles, Ta; gray circles, S; open circles, Br.

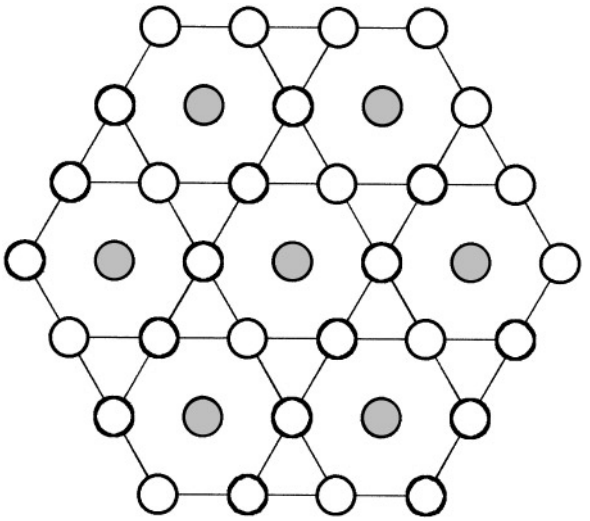

FIG. 2. Ordering pattern formed by the anion layers in Ta_3SBr_7 and Nb_3SBr_7. The positions of S or Br1 within the layers are shown as shaded circles.

atoms are shown as small black circles. Bonds are omitted for clarity. The two one-slab structures are generated as follows:

1. Perfect superposition of like ordered anion sheets: each A (or B) sheet stacks directly over all other A (or B) sheets (perfect … ABAB … pattern). Referring to Fig. 3, and focusing on any sulfur atom in a "B" sheet, this corresponds to all sulfur atoms in every "B" sheet stacking directly above the sulfur atoms in all other "B" sheets, in essence "lining up" along the stacking direction. This stacking sequence generates the previously discovered Nb_3SBr_7 type. Successive $^2_\infty[Nb_3SBr_7]$ slabs are related to one another simply by a lattice translation in the [001] direction (see Fig. 3), leading to the high-symmetry small hexagonal cell, space group $P3m1$ (the simplest structure of all M_3QX_7 compounds), with one formula unit per unit cell.

2. Shifting of every other slab such that the "A" and "B" sheets in alternating slabs have moved to any one of the six available nearest neighbor "A" and "B" sites, respectively (ABA′B′). Again referring to Fig. 3 and focusing on any sulfur atom in a "B" sheet, this corresponds to sulfur atoms in alternate slabs situated above any one of the six adjacent "B" sites (light atoms) specified by arrows. The Ta_3 clusters follow the position of the sulfur. (Conceptually "moving" the appropriate layers in any of the six directions specified by the arrows in Fig. 3 yields the same three-dimensional structure, but with a different relative orientation of the unit cell.) This stacking sequence generates the new monoclinic Ta_3SBr_7 structure type, where the cluster pattern is such that successive slabs are related to one another by the stacking vector $[\frac{1}{2}\mathbf{b} + \mathbf{c}]$, with two formula units per unit cell.

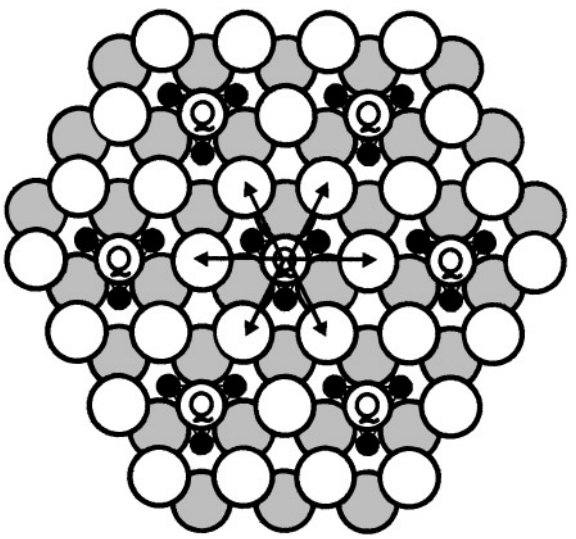

FIG. 3. A single $^2_\infty[M_3QX_7]$ slab. Large gray circles: "A" layer (Br1, Br3, Br5). Large open circles: "B" layer (Br2, Br4, S (= Q, labeled). Small black circles: M_3 clusters. Arrows indicate shifts of alternate slabs that generate the Ta_3SBr_7 structure while maintaining overall ⋯AB⋯ stacking. See text for complete description.

A multitude of stacking modes involving multislab stacking and alternate orientations of the Ta_3Q_{cap} fragments is of course possible, but *within the constraint of one slab per unit cell*, these ordered sheets can stack only in the two unique ways described above. All other stacking possibilities result in a structure containing at least two slabs per unit cell. Why this is so can be seen by considering the following requirements for a one-slab M_3QX_7 structure, which both must be satisfied simultaneously.

1. …AB… stacking of the anion sheets: clearly, more complicated stacking patterns (e.g. ABAC, ABCB) require a larger repeat unit.
2. Noncentrosymmetry: for M_3QX_7 systems, this implies unidirectional orientation of all M_3Q_{cap} fragments. If the M_3Q_{cap} fragments alternate direction throughout the structure, again the repeat unit must incorporate fragments from at least two slabs.

The simplicity of having only two stacking type choices obviously disappears when the possibility of more than one slab per unit cell and alternate orientations of the M_3Q_{cap} fragments are allowed. Allowing two slab per unit cell stacking, the number of possible structure types increases to 24. This number includes the one-slab Nb_3SBr_7 and Ta_3SBr_7 types, which can be thought of as a special subset of larger two-slab set. Only three two-slab structures have been found: the Nb_3SeI_7, Nb_3TeBr_7, and α-Nb_3Cl_8 types. In a manner similar to how the structure of Ta_3SBr_7 was derived from that of Nb_3SBr_7 (see above), the structures of

these 24 variants can also be derived. As proof of the existence of the 24 two-slab types, consider the following. Six nonequivalent sites surround each anion sheet atom. Two orientations of the Ta_3Q_{cap} units relative to those in the adjacent slabs ("ferroelectric" and "antiferroelectric") are possible. Finally, there are two possible unique rotational conformations of the slabs relative to one another (identity + 6-fold rotation of the adjacent slab). Thus, $6 \times 2 \times 2 = 24$ possible types. Of these 24, 12 display chemically unreasonable anion stacking sequences, involving directly superimposed atom sheets (i.e., an AA sequence), giving rise to trigonal prismatic sites in the van der Waals gap. Such stacking has never been observed in these systems, or indeed in any system without an atom in the trigonal prismatic holes to hold the layers in this position (e.g., MoS_2). After discarding the 12 structures with ABBA, ABBC, or ABCA stacking, 12 feasible types remain. Representations of these 12 types are given in Fig. 4. In this figure, only the spatial relationship of two metal triangles situated in adjacent slabs is shown in projection down the stacking direction. A hexagonal unit cell is indicated in dashed line for comparison with Nb_3SBr_7. The anion sheet stacking sequence is given next to each projection, and the projections are divided into two classes, ferroelectric (unidirectional orientation of the Ta_3Q_{cap} dipole) and antiferroelectric (the Ta_3Q_{cap} dipole alternates direction from slab to slab).

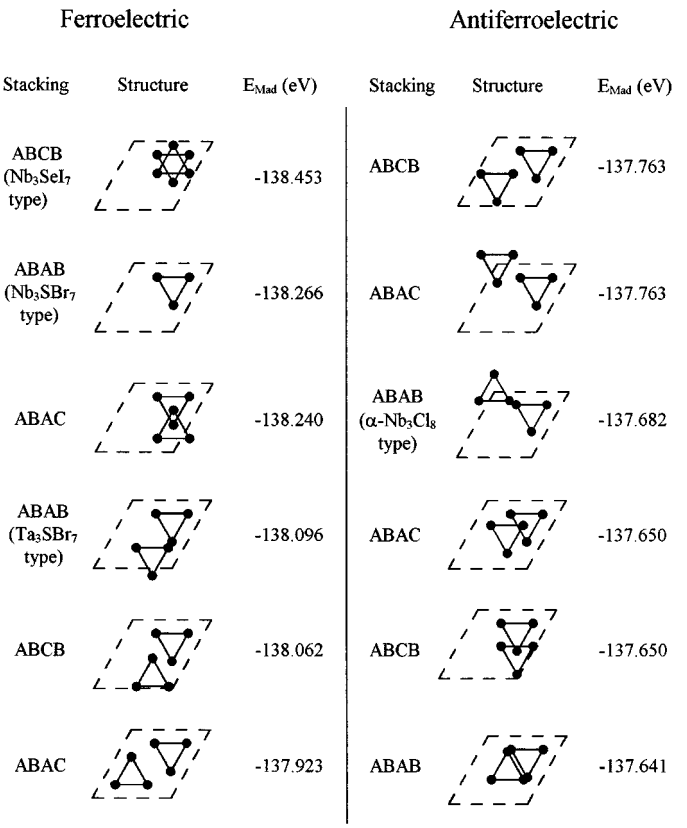

FIG. 4. Partial projections of the twelve structures used in lattice energy calculations. Positions of the metal cluster sites in adjacent slabs are shown. Anion stacking sequences are given to the left of each projection, and calculated Madelung energies to the right.

In order to compare the relative energies of the possible two-slab structures, lattice energy calculations were performed. The Madelung energies were evaluated, and Born–Mayer repulsion terms were included to probe for small repulsive interactions between tantalum atoms which might drive adoption of a particular type. The hypothetical structures mimic actual $^2_\infty[M_3QX_7]$ slabs as far as reasonably possible. Within the slabs, however, slight deviations from the observed bond lengths were introduced due to the use of perfect close-packed anion sheets in the calculations. Actual M_3QX_7 compounds show slight disruptions due to metal clustering, as discussed further later. Ta–Ta and Ta–S distances were set equal to those observed in Ta_3SBr_7, and all others were within 0.1 Å of the observed distances. The distance between slabs (the van der Waals gap) was taken from that observed in Ta_3SBr_7. These slabs were "stacked" to produce the twelve structures investigated. Since the slabs are identical, the calculated energies reflect interactions through the van der Waals gap rather than within the slabs.

Initially, Madelung energies alone were evaluated. These are listed in Fig. 4. The results show a clear sorting of the structures into two classes, ferroelectric and antiferroelectric. In all cases, the six ferroelectric structures were favored (more negative Madelung energies). Such an arrangement maximizes the distance between the sulfurs, reducing strong repulsion between the "hard" S^{2-} anions. Further inspection of the six favorable ferroelectric structure also suggests a preference for the slabs to align such that the more highly charged chalcogen anion be as near as possible to the metal cations in the adjacent slab. Interestingly, the only observed M_3QX_7 compounds that form with an antiferroelectric structure are M_3QCl_7 (M = Nb, Ta; Q = Se, Te), implying greater importance of the Madelung term for the bromides and iodides, as suggested earlier (3).

Next, the Born–Mayer repulsion term was taken into account. Including this term changed the energetic ordering of the structures, making Ta_3SBr_7 the most favored of the *observed* structure types, but still calculated to be energetically unfavorable with respect to three hypothetical structures.

The failure of these calculations to predict the Ta_3SBr_7 type as the most favorable of the twelve structures is not too disturbing, though, since the energetic separation of the lowest energy structures is rather small (ca. 0.4 eV on a scale of > 100 eV).

The stacking mode in Ta_3SBr_7 prohibits the possibility of hexagonal symmetry. The threefold axis and two of the three mirror planes centered on the M_3SBr_7 cluster unit in the hexagonal case are lost: the local cluster point symmetry drops from C_{3v} to C_s, with the one remaining mirror plane

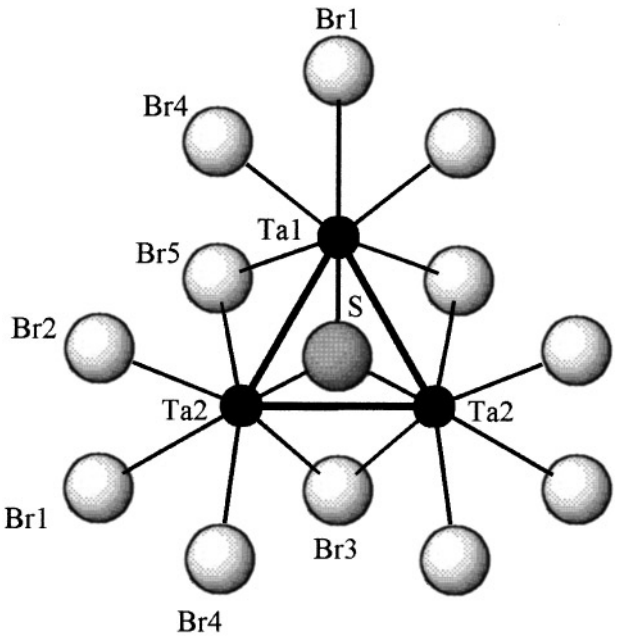

FIG. 5. Ta_3SBr_7 cluster atom labeling scheme. A mirror plane bisects Br1, Ta1, S, and Br3. Small black circles, Ta; large gray circle, S; large open circles, Br.

TABLE 3
Comparison of Bond Distances in Ta_3SBr_7 and Nb_3SBr_7 (Å) and Selected Bond Angles in Ta_3SBr_7 (deg)

Ta_3SBr_7		Nb_3SBr_7	
Ta1–Ta2	2.862(2)	Nb–Nb	2.896
Ta2–Ta2	2.864(2)		
Ta1–S	2.44(2)	Nb–S	2.410
Ta2–S	2.36(1)		
Ta1–Br1	2.793(7)	Nb–Br1	2.804
Ta2–Br1	2.801(4)		
Ta1–Br5	2.545(5)		
Ta2–Br5	2.532(4)	Nb–Br2	2.544
Ta2–Br3	2.545(5)		
Ta1–Br4	2.678(5)		
Ta2–Br4	2.681(5)	Nb–Br3	2.687
Ta2–Br2	2.673(3)		
(Horizontal lines above separate sets of bonds rendered inequivalent by the lower symmetry of Ta_3SBr_7)			
Ta2–Ta1–Ta2	60.04(6)	Ta1–Br1–Ta2	97.6(2)
Ta1–Ta2–Ta2	59.98(3)	S–Ta1–Br1	165.1(4)
Ta1–S–Ta2	73.2(4)	S–Ta2–Br1	162.7(3)
Ta2–S–Ta2	74.7(4)	Br4–Ta2–Br5	162.1(1)
Ta1–Br5–Ta2	68.6(1)	Br4–Ta1–Br5	162.2(2)
Ta2–Br3–Ta2	68.5(1)		

dividing the cluster into two sets of crystallographically inequivalent atoms. The cluster unit and atom labeling scheme are shown in Fig. 5. However, the slight distortions away from C_{3v} cluster symmetry result simply from a mild (in fact nearly negligible) "relaxation" of the structure when hexagonal symmetry constraints are removed upon lowering to monoclinic symmetry. Within (or very close to within) experimental error, all Ta–Ta and Ta–S bond distances are equivalent: Ta1–Ta1, 2.862(2) Å; Ta1–Ta2, 2.864(2) Å; Ta1–S, 2.44(2) Å; Ta2–S, 2.36(1) Å. Ta–Br distances follow this trend also. The triangular cluster is still nearly equilateral: $\angle$Ta1 = 60.04(6)°, $\angle$Ta2 = 59.98(3)°. Other relevant bond distances and angles are listed in Table 3.

In order to approach each other closely enough to achieve the Ta–Ta bond distances mentioned above, the tantalum atoms are displaced from the centers of their octahedral sites toward the centroid of the resultant cluster. These displacements affect the surrounding anion layer network. The atom in the anion layer ("B" sheet) directly above the three clustered metals (the capping sulfur atom) is "squeezed" up into the van der Waals gap to minimize repulsion from the tightly bound triangle beneath it. Simultaneously, a halide (Br1) is drawn into the metal atom layer in compensation for the space left by the displaced metal atoms. The result of these anion displacements (driven by the formation of the metal triangle) is a topographical pattern of elevations on the top side of each $^2_\infty[Ta_3SBr_7]$ slab and indentations on the underside. These corrugations occur in all M_3QX_7 compounds, as well as in Nb_3X_8. In the parent $Cd(OH)_2$ structure, of course no metal–metal bonding exists; each Cd atom sits exactly in the center of its octahedral hole, and the anion layers are flat. Recent atomic force microscopy (AFM) experiments performed on samples of Ta_3TeI_7 (14) did in fact reveal such atomic corrugations on both surfaces of the $^2_\infty[Ta_3TeI_7]$ slabs. Earlier AFM experiments on the binary halides Nb_3X_8 (X = Cl, Br, I) provided images of the $^2_\infty[Nb_3X_8]$ slab surface containing the X_{cap} atom, where a similar elevation of the capping halide was observed (15).

In Ta_3SBr_7, the sulfur atoms lie 0.297 Å above the surrounding Br2 + Br4 layer, and Br1 is lifted 0.302 Å into the metal layer. It is interesting to note that in Ta_3SBr_7, successive slabs are stacked so that the "bumps" caused by the protruding S atoms on the top side of a slab correlate with the indentations caused by the lifting of Br1 into the underside of the adjacent slab. However, it is unlikely that this is the reason for the particular stacking mode in Ta_3SBr_7. Nb_3SBr_7 shows the same bumps/depressions, but crystallizes so that the sulfurs directly about a flat surface. Furthermore, no preferred fitting is observed even in compounds where, because of different relative sizes of chalcogen and halide, the bumps and depressions are even more pronounced. For example, in Ta_3TeI_7, the large Te^{2-} anions protrude 0.55 Å above the surrounding iodide layer, yet no correlation of these contours is observed. In Nb_3TeCl_7 (3) and Ta_3TeCl_7 (16), where the chalcogen/halogen size ratio is largest, a centrosymmetric structure forms where the

elevated Te atoms share the same van der Waals gap space.

The above considerations underscore the subtlety of the factors governing the formation of a particular polytype: the effect of entropic terms and hard-to-control experimental details like internal pressure in the reaction tube, unwanted (but ever-present) temperature gradients, and lack of knowledge about nucleation and crystal-growth mechanisms, all of which are difficult to quantify. Most likely, an interplay between very small energetic and entropic effects beyond the scope of our calculations determines the various stackings of the weakly interacting $^{2}_{\infty}[M_3QX_7]$ slabs in such layered compounds. This suggests that, upon finding the right conditions, polytypism might be observed in these systems. In an attempt to investigate temperature effects on the formation of different poltypes, crystals of Nb_3SBr_7 were grown in our lab at 450°C, 600°C and the reported 800–750°C transport conditions. Nb_3SBr_7 was chosen because Ta_3SBr_7 thermally decomposes into Ta_6Br_{15}, $TaBr_5$, and TaS_2 above ca. 575°C, so its temperature stability region offers less flexibility than does Nb_3SBr_7. Several Nb_3SBr_7 crystals from each reaction temperature were chosen. All reproduced the published hexagonal structure, as determined by single-crystal X-ray diffraction. Furthermore, no indication of a different stacking variant is seen in Guinier powder X-ray diffraction patterns of many additional crystal samples, or of bulk powders.

Tantalum and niobium are well-known for their often indistinguishable behavior at moderate temperatures, and the departure of Ta_3SBr_7 from the structural model set by Nb_3SBr_7 is unusual. This sulfide bromide pair offers an interesting opportunity for a mixed-metal study, namely $Nb_xTa_{3-x}SBr_7$ ($0 \leq x \leq 3$). Which of the two structures will be preferred? Will the relative amounts of each metal play a role? Although a tantalum-rich system might be expected to adopt the Ta_3SBr_7 structure and vice versa, a composition around $Nb_{1.5}Ta_{1.5}SBr_7$ might yield unexpectd results. Preliminary results from such $Nb_{1.5}Ta_{1.5}SBr_7$ reactions, however, have given only tantalum-rich single crystals. All crystals selected thus far have all refined to a composition near Ta_2NbSBr_7, and verify that at least at this Ta/Nb ratio, the Ta_3SBr_7 type is indeed adopted. Further efforts at growing crystals in this system with varying Ta/Nb compositions are underway.

REFERENCES

1. S. Furuseth, W. Hönle, G. J. Miller, and H. G. von Schnering, *in* "9th International Conference of Transition Elements, Abstracts." Royal Society of Chemistry, London, 1988.
2. G. J. Miller, *J. Alloys Compds.* **229,** 93 and references therein (1995).
3. G. J. Miller, *J. Alloys Compds.* **217,** 5 (1995).
4. H. G. von Schnering, H. Wöhrle, and H. Schäfer, *Naturwissenschaften* **48,** 159 (1961).
5. A. Simon and H. G. von Schnering, *J. Less-Common Met.* **11,** 31 (1966).
6. G. V. Khvoryjkh, A. V. Shevelkov, V. A. Dolgikh, and B. A. Popovkin, *J. Solid State Chem.* **120,** 311 (1995).
7. G. J. Miller, J. Lin, and C.-S. Lee, manuscript in preparation. [See also Ref. (2)].
8. M. D. Smith and G. J. Miller, *J. Am. Chem. Soc.* **118,** 12238 (1996).
9. G. M. Sheldrick, "SHELXS-86." Univ. Göttingen, Germany, 1986.
10. "TEXSAN: Single Crystal Structure Analysis Software," Version 5.0. Molecular Structure Corp., The Woodlands, TX, 1989.
11. N. Walker and D. Stuart, *Acta Crystallogr. A* **39,** 158 (1986).
12. S. C. Bevan and D. F. C. Morris, *J. Chem. Soc.*, 516 (1960).
13. J. M. Ziman, "Principles of the Theory of Solids," p. 39. Cambridge Univ. Press, London, 1964.
14. P. Schmidt and M.-H. Whangbo, personal communication.
15. S. N. Maganov, P. Zönnchen, H. Rotter, H.-J. Cantow, G. Thiele, J. Ren, and M.-H. Whangbo, *J. Am. Chem. Soc.* **115,** 2495 (1993).
16. M. D. Smith and G. J. Miller, unpublished research.